Journal of
Nanoscience and Nanotechnology
Vol. 5, 1532–1536, 2005

Polyol-Mediated Synthesis and Photoluminescent Properties of Ce^{3+} and/or Tb^{3+}-Doped $LaPO_4$ Nanoparticles

Zhenling Wang,[1] Zewei Quan,[1] Jun Lin,[1,*] and Jiye Fang[2]

[1] *Key Laboratory of Rare Earth Chemistry and Physics, Changchun Institute of Applied Chemistry, Chinese Academy of Sciences, Changchun 130022, and Graduate School of the Chinese Academy of Sciences, Beijing 100049, P. R. China*

[2] *Department of Chemistry and Advanced Materials Research Institute, University of New Orleans, New Orleans, LA 70148, USA*

Rare-earth ion (Ce^{3+}, Tb^{3+}) doped $LaPO_4$ nanoparticles were prepared by the polyol method and characterized by X-ray diffraction (XRD), field emission scanning electron microscopy (FE-SEM), UV–vis absorption spectroscopy, photoluminescence (PL) spectroscopy, and lifetimes. The results of XRD indicate that the as-prepared nanoparticles are well-crystallized at 160 °C and assigned to the monoclinic monazite structure of the $LaPO_4$ phase. The obtained $LaPO_4$:Ce^{3+}, Tb^{3+} nanoparticles are spherical with narrow size distribution and average size of 20 nm. The doped rare-earth ions show their characteristic emission in $LaPO_4$ nanoparticles, i.e., Ce^{3+} 5d–4f and Tb^{3+} $^5D_4$–^7F_J (J = 6–3) transitions, respectively. The optimum doping concentration for Tb^{3+} in $La_{0.8-x}Ce_{0.2}Tb_xPO_4$ nanoparticles is determined to be 15 mol% ($x = 0.15$). The luminescence decay curves of Ce^{3+} in $LaPO_4$:Ce^{3+} and $LaPO_4$:Ce^{3+}, Tb^{3+} nanoparticles present a single-exponential behavior, and the lifetimes (τ) of Ce^{3+} decrease with increasing Tb^{3+} concentrations (at the constant Ce^{3+} concentration) in $LaPO_4$:Ce^{3+}, Tb^{3+} nanoparticles due to the energy transfer from Ce^{3+} to Tb^{3+}. The energy-transfer efficiency from Ce^{3+} to Tb^{3+} was calculated, which depends on the doping concentrations of Tb^{3+} if the concentration of Ce^{3+} is fixed.

Keywords: Polyol Method, Nanoparticle, $LaPO_4$, Rare-Earth Ion, Photoluminescence.

RESEARCH ARTICLE

1. INTRODUCTION

Nanometric luminescent materials have some different properties from those of the bulk because of a high surface-to-volume ratio and the quantum confinement effect of nanoscale materials.[1] They have attracted a great deal of interest as components in light-emitting diodes (LEDs), displays, biological assays, and optoelectronic devices with nanometer dimensions and as a light source in zero-threshold lasers.[2] Recently, most studies on nanometric luminescent materials have been focused on semiconductor nanocrystals.[3–7] However, a significant amount of research has been devoted to lanthanide (III)-doped oxide materials.[8–16]

The liquid-phase synthesis in high boiling coordinating solvents is a versatile method for preparing a variety of colloidal nanocrystals. Due to the binding of the solvent molecules to the particle surface, well-separated nanoparticles can be obtained. A type of liquid-phase synthesis method that resulted in precipitation while heating suitable precursors in a multivalent and high boiling alcohol (e.g., diethylene glycol, DEG, bp 246 °C) is the so-called polyol method.[12] This method is comparably easy to perform and well-suited for the preparation of 30–200 nm spherical particles. There are several merits for this method: First, the high temperatures and nonaqueous environment allow a direct synthesis of oxides instead of hydroxides. Second, normally well-crystallized materials are realized due to the high temperature during the synthesis; moreover, the high boiling temperature should make it possible to obtain colloids with different particle sizes when varying the synthesis temperatures. Third, the polyol medium efficiently complexes the surface of the particles,

*Author to whom correspondence should be addressed.

1533-4880/2005/5/1532/005 doi:10.1166/jnn.2005.319

so the particles growth is limited and an agglomeration of particles is prevented. Finally, the reductive properties of the alcohol allow for direct decomposition of the metal precursor under high reaction temperatures without adding any catalysts.[12, 13, 17–19] So far, the polyol method has been successfully used to prepare a large variety of materials, including elemental metals and alloys,[19, 20] oxides,[18, 21–23] sulfides,[17] phosphates,[24] inorganic pigments,[25, 26] and rare earth-based luminescent materials.[12, 13]

Lanthanum phosphate ($LaPO_4$, monazite) has been shown to be a useful host lattice for rare earth ions to produce phosphors emitting a variety colors.[27–29] $LaPO_4$ doped with cerium and terbium is a highly efficient and commercially applied lamp phosphor.[30] In this paper, we report on the polyol method synthesis of lanthanide (Ce^{3+}, and Tb^{3+})-doped $LaPO_4$ nanoparticles. The PL properties and the energy transfer phenomena of the resulted nanoparticles are discussed.

2. EXPERIMENTAL DETAILS

Ce^{3+} and/or Tb^{3+} doped $LaPO_4$ nanoparticles were prepared by the polyol method as described previously.[12, 24] Typically, stoichiometric amounts of La_2O_3 (99.99%), Tb_4O_7 (99.99%), and $Ce(NO_3)_3 \cdot 6H_2O$ (99.99%) were dissolved in diluted nitric acid (HNO_3, analytical reagent, A.R.), and then the water in above solutions was distilled off by heating. The resulting nitrates, a stoichiometric amount of $(NH_4)_2HPO_4$ (99%, A.R.) and a desirable amount of DEG (98%, A.R.) were mixed together to make the metal ion concentration be 0.02 mol/L, then transferred to a round-bottomed flask. The mixture was heated in a silicon oil bath under vigorous stirring with a flow of nitrogen and the temperature of the solution was increased to 160 °C. Then the suspension was cooled to room temperature and diluted with twofold excess of ethanol and the solid was separated by centrifugation. In order to remove residual DEG, the solid was twice resuspended in ethanol and centrifuged again. Finally, the solid was dried at 60 °C under vacuum.

X-ray diffraction (XRD) was carried out on a Rigaku-Dmax 2500 diffractometer with Cu Kα radiation (λ = 0.15405 nm). An accelerating voltage of 40 kV and emission current of 200 mA were used. SEM micrographs were obtained by using a field emission scanning electron microscope (FE-SEM, XL30, Philips). The excitation and emission spectra were taken on an F-4500 spectrophotometer equipped with a 150-W xenon lamp as the excitation source. The luminescence lifetimes of Tb^{3+} were measured with a SPEX 1934D phosphorimeter using a 7-W pulse xenon lamp (pulse width = 3 μs) as the excitation source. The luminescence lifetimes of Ce^{3+} were measured with a Lecroy Wave Runner 6100 digital oscilloscope (1 GHz) using 275-nm lasers (pulse width = 4 ns) as the excitation source (Continuum Sunlite OPO). All the measurements were performed at room temperature.

3. RESULTS AND DISCUSSION

3.1. Phase Formation and Morphology

The phase structure and morphology of the as-prepared samples were investigated by XRD and FE-SEM techniques, respectively. Figure 1 shows the XRD patterns of $La_{0.65}Ce_{0.2}Tb_{0.15}PO_4$ nanoparticles (the starting concentration of metal precursors is 0.02 mol/L). The result of XRD indicates that the nanoparticles of $La_{0.65}Ce_{0.2}Tb_{0.15}PO_4$ are well-crystallized and the patterns are in good agreement with the monoclinic monazite structure known from bulk $LaPO_4$ powders (JCPDS Card No. 84-0600). Lucas et al. have reported that the phase transformation from the hexagonal to monoclinic structure was observed at about 600 °C for $LaPO_4$ powders,[31] whereas under our experimental conditions, the monoclinic structure of $LaPO_4$:Ce^{3+}, Tb^{3+} nanoparticles can form in DEG solution at a temperature as low as 160 °C. The nanocrystallite size can be estimated from the Scherrer equation, $D = 0.90\lambda/\beta\cos\theta$, where D is the average grain size, λ is the X-ray wavelength (0.154 05 nm), and θ and β are the diffraction angle and full width at half-maximum (FWHM) of an observed peak, respectively.[32] The strongest peak (012) at $2\theta = 31.2°$ was used to calculate the average crystallite size (D) of $LaPO_4$:Ce^{3+}, Tb^{3+} nanoparticles. The estimated average crystallite size of $La_{0.65}Ce_{0.2}Tb_{0.15}PO_4$ particles is around 15 nm.

Figure 2 shows the FE-SEM image of $La_{0.65}Ce_{0.2}Tb_{0.15}PO_4$ nanoparticles. From this figure it can be seen clearly that these nanoparticles are spherical with a narrow size distribution. The average size of these particles is about 20 nm, slightly larger than that calculated from the Scherrer equation. This is not surprising because smaller nanograins contribute more to the broadening of the diffraction peaks as reported previously.[32]

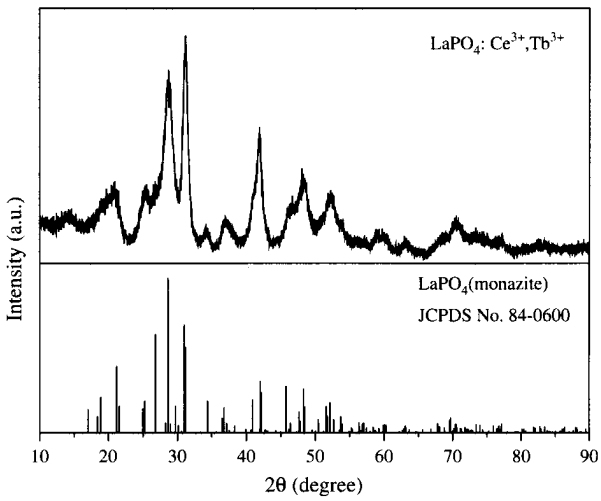

Fig. 1. X-ray diffraction pattern of $La_{0.65}Ce_{0.2}Tb_{0.15}PO_4$ nanoparticles and the standard data for $LaPO_4$ (JCPDS card No. 84-0600).

RESEARCH ARTICLE

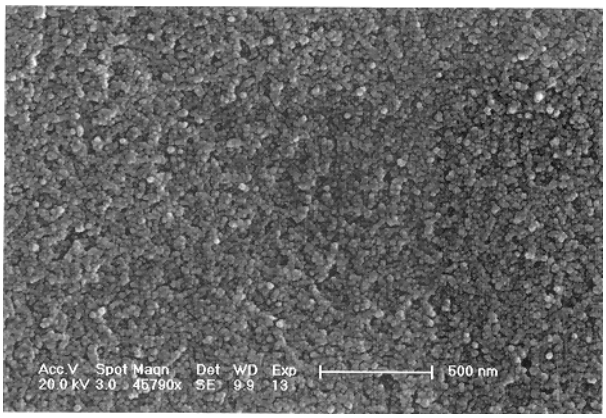

Fig. 2. FE-SEM image of $La_{0.65}Ce_{0.2}Tb_{0.15}PO_4$ nanoparticles.

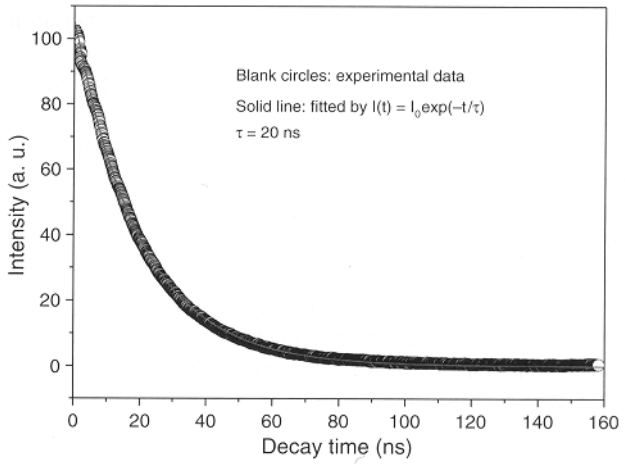

Fig. 4. Decay curve of Ce^{3+} luminescence (341 nm) in $La_{0.8}Ce_{0.2}PO_4$ nanoparticles ($\lambda_{ex} = 275$ nm).

3.2. Photoluminescence Properties

$LaPO_4$:Ce^{3+}. Ce^{3+}-doped $LaPO_4$ nanoparticles show an emission in the UV region. Figure 3 gives the absorption (a), excitation (b), and emission (c) spectra for $La_{0.8}Ce_{0.2}PO_4$ nanoparticles. The emission spectrum (Fig. 3c) of Ce^{3+} includes a broad band with a maximum at 341 nm, which is assigned to the parity allowed transitions of the lowest component of the ^2D state to the spin–orbit components of the ground state of Ce^{3+}. Note that in bulk[33] and thin film[34] of $LaPO_4$:Ce^{3+}, two well-resolved emission peaks at 318 and 336 nm are observed due to the ground-state splitting of Ce^{3+}($^2F_{5/2}$, $^2F_{7/2}$). This splitting for Ce^{3+} in the current $LaPO_4$ nanoparticles cannot be resolved clearly due to the broadening of spectral lines induced by the small size effects. Monitored with the emission wavelength (341 nm), the obtained excitation spectrum (Fig. 3b) consists of a broad and strong peak with a maximum at 275 nm and three small shoulder peaks at 260, 241, and 217 nm, which correspond to the transitions from the ground state $^2F_{5/2}$ of Ce^{3+} to the different components of the excited Ce^{3+} 5d states split by the crystal field, respectively.[34] The short wavelength component of the Ce^{3+} emission band has a low intensity due to self-absorption for high Ce^{3+} concentrations.[33] The absorption spectrum (Fig. 3c) of $La_{0.8}Ce_{0.2}PO_4$ nanoparticles dispersed in ethylene glycol solution shows two absorption peaks at 273 and 257 nm for Ce^{3+}, basically in agreement with the excitation spectrum.

Figure 4 shows the luminescence decay curve of Ce^{3+} in $La_{0.8}Ce_{0.2}PO_4$ nanoparticles. This curve can be well-fitted into a single exponential function as $I = I_0 \exp(-t/\tau)$ (τ is $1/e$ lifetime of the Ce^{3+} ion). The lifetime of Ce^{3+} is determined to be 20 ns by this fitting.

$LaPO_4$:Ce^{3+}, Tb^{3+}. The $LaPO_4$ nanoparticles codoped with Ce^{3+} and Tb^{3+} ions show a strong green emission under short UV excitation. Figure 5 gives the absorption (a), excitation (b), and emission (c) spectra for $La_{0.65}Ce_{0.2}Tb_{0.15}PO_4$ nanoparticles. The excitation spectrum (Fig. 5b)

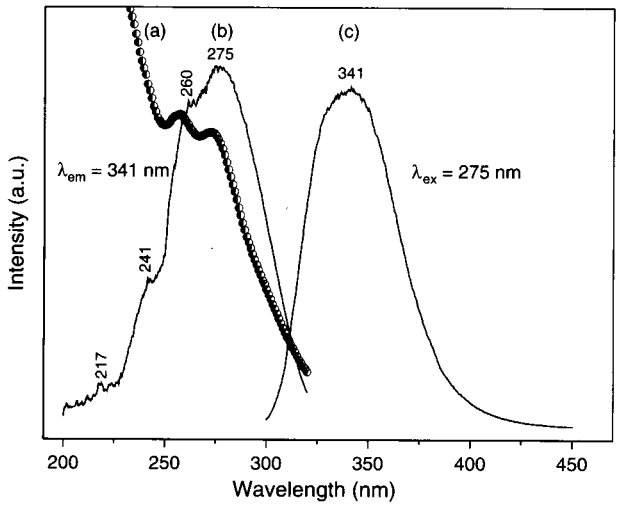

Fig. 3. Absorption (a), excitation (b), and emission (c) spectra of $La_{0.8}Ce_{0.2}PO_4$ nanoparticles.

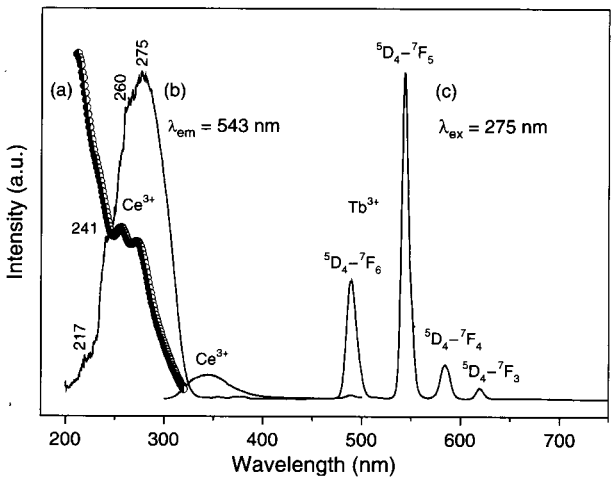

Fig. 5. Absorption (a), excitation (b), and emission (c) spectra of $La_{0.65}Ce_{0.2}Tb_{0.15}PO_4$ nanoparticles.

RESEARCH ARTICLE

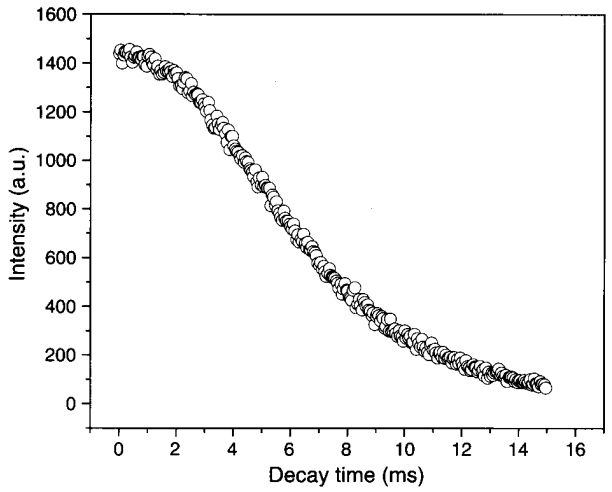

Fig. 6. Decay curve of Tb^{3+} ($^5D_4$–$^7F_5$ at 543 nm) luminescence in $La_{0.65}Ce_{0.2}Tb_{0.15}PO_4$ nanoparticles.

monitored with the 543-nm emission ($^5D_4$–$^7F_5$) of Tb^{3+} is identical with that of $La_{0.8}Ce_{0.2}PO_4$ (Fig. 3b). The absorption spectrum (Fig. 5a) of $La_{0.65}Ce_{0.2}Tb_{0.15}PO_4$ nanoparticles dispersed in ethylene glycol solution shows two strong absorption peaks at 257 and 273 nm for the Ce^{3+}, agreeing well with that of $La_{0.8}Ce_{0.2}PO_4$ nanoparticles (Fig. 3a). Excitation into the Ce^{3+} band at 275 nm yields both the weak emission of Ce^{3+} (300–400 nm) and strong emission of Tb^{3+} (450–650 nm). This indicates that an energy transfer from Ce^{3+} to Tb^{3+} occurs in the $La_{0.65}Ce_{0.2}Tb_{0.15}PO_4$ nanoparticles, as observed in the bulk powder materials[35] and colloids of $LaPO_4$:Ce, Tb.[11] The emission of Tb^{3+} is due to transitions between the excited $^5D_4$ state and the ^7F_J ($J = 6$–3) ground states of Tb^{3+} ions. No emission from the higher $^5D_3$ level is observed due to the cross relaxation effect at the high Tb^{3+} concentration.[34]

Figure 6 shows the luminescence decay curve of Tb^{3+} in $LaPO_4$:Ce^{3+}, Tb^{3+} nanoparticles. Unlike the single-exponential luminescence decay of $LaPO_4$:Ce^{3+} nanoparticles, the luminescence decay curve of Tb^{3+} in $La_{0.65}Ce_{0.2}Tb_{0.15}PO_4$ nanoparticles deviates from single-exponential behavior. This nonexponential luminescence kinetics confirmed further that an energy transfer from Ce^{3+} to Tb^{3+} occurs in the nanoparticles of $LaPO_4$:Ce^{3+}, Tb^{3+}.[10, 34]

Energy Transfer from Ce^{3+} to Tb^{3+} in $LaPO_4$ Nanoparticles. Energy transfer is an important process in the luminescence phenomena for solid-state luminescent materials. Optical transitions within $4f^n$ configurations of Tb^{3+} are so strongly forbidden that they appear in the absorption spectra as very weak. However, excitation resulting in high light output can be achieved by exciting a different ion (sensitizer, i.e., Ce^{3+}) with an optically allowed transition which transfers the excitation energy to the rare earth activator (i.e., Tb^{3+}).[36] So the energy-transfer processes from Ce^{3+} to Tb^{3+} can enhance the Tb^{3+} green emission in co-doped $LaPO_4$ phosphors. To confirm the energy-transfer process from Ce^{3+} to Tb^{3+} further, the lifetimes

Table I. Lifetimes (τ) of Ce^{3+}, emission intensities of Ce^{3+} and Tb^{3+}, as well as energy transfer efficiency (η_{ET}) from Ce^{3+} to Tb^{3+} in $La_{0.8-x}Ce_{0.2}Tb_xPO_4$ ($x = 0$–0.25) nanoparticles upon excitation into the Ce^{3+} at 275 nm.

	x						
	0	0.01	0.05	0.10	0.15	0.20	0.25
$\tau(Ce^{3+})$, ns	20.0	17.5	16.7	15.3	14.4	9.5	9.1
$I(Ce^{3+})$, arb. unit	815	504	434	356	281	158	134
$I(Tb^{3+})$, arb. unit		485	2236	2672	3759	3250	2805
η_{ET} (%)		38.2	46.75	56.32	65.52	80.61	83.56

of Ce^{3+} in $La_{0.8-x}Ce_{0.2}Tb_xPO_4$ ($x = 0$–0.25) nanoparticles were measured, as listed in Table I. The lifetimes (τ) of Ce^{3+} decrease with increasing the Tb^{3+} concentrations, further indicating that an energy transfer from Ce^{3+} to Tb^{3+} occurs in the $LaPO_4$:Ce^{3+}, Tb^{3+} nanoparticles.[37]

Energy level scheme of $LaPO_4$:Ce^{3+}, Tb^{3+} with optical transitions and energy transfer processes between Ce^{3+} and Tb^{3+} is depicted in Figure 7.[11] First Ce^{3+} ions were excited by UV light excitation; subsequently, energy transfer takes place from Ce^{3+} to Ce^{3+} and then from 5d (Ce^{3+}) to the excitation high levels of Tb^{3+} ($4f^n$), followed by rapid internal conversion to the $^5D_4$ level of Tb^{3+}, which decays nonradiatively to various lower levels of ^7F_J ($J = 0, 1, 2, 3, 4, 5$, and 6). The energy levels of Tb^{3+} ($4f^n$) are suitable for the energy transfer to take place from the allowed Ce^{3+} emission of (f–d) upon excitation with UV light.[33, 36] That the Ce^{3+}–Ce^{3+} energy diffusion process should play a role in the energy-transfer process appears reasonable in view of the involvement of parity allowed d–f transition moments.[35] The Tb^{3+} ion acts as the terminal of the energy-transfer processes in the $LaPO_4$:Ce^{3+}, Tb^{3+} system.

The energy transfer efficiency (η_{ET}) from Ce^{3+} to Tb^{3+} depends strongly on Tb^{3+} doping concentrations in $La_{0.8-x}Ce_{0.2}Tb_xPO_4$ nanoparticles. The energy-transfer

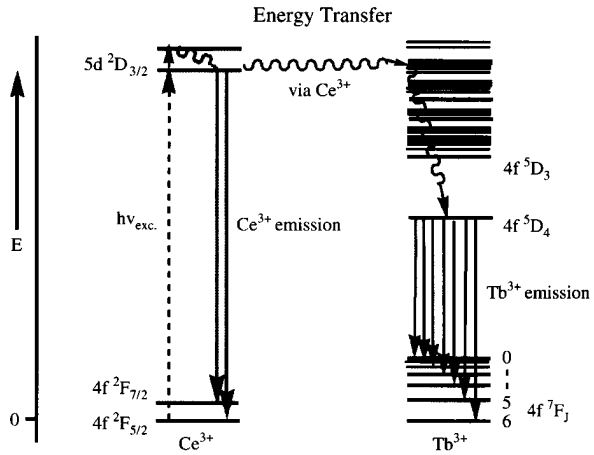

Fig. 7. Energy level scheme of $LaPO_4$:Ce^{3+}, Tb^{3+} with optical transitions and energy-transfer processes.

efficiency from a donor (Ce^{3+}) to an acceptor (Tb^{3+}) can be calculated according to the formula $\eta_{ET} = 1 - I_d/I_{d0}$, where I_d and I_{d0} are the corresponding luminescence intensities of the donor (Ce^{3+}) in the presence and absence of the acceptor (Tb^{3+}) for the same donor (Ce^{3+}) concentration, respectively.[35] We investigated systematically the energy-transfer efficiencies from Ce^{3+} to Tb^{3+} in $La_{0.8-x}Ce_{0.2}Tb_xPO_4$ ($x = 0.01$–0.25) nanoparticles and the results are listed in Table I. It is known from Table I that with increasing Tb^{3+} concentration, the energy transfer efficiency from Ce^{3+} to Tb^{3+} increases gradually. This is because the energy-transfer probability from Ce^{3+} to Tb^{3+} is proportional to R^{-6} (R is the average distance between Ce^{3+} and Tb^{3+}).[10] When the x value is equal to 0.25, η_{ET} reaches as high as 83.6%, but the emission of Tb^{3+} is not the strongest because concentration quenching has occurred at this high concentration. The strongest emission was observed when the x value was 0.15 with an energy-transfer efficiency of 65.5% from Ce^{3+} to Tb^{3+}. This effect of Tb^{3+} doping concentrations on the energy-transfer efficiency and luminescence intensities are similar to what we observed in the nanocrystalline $LaPO_4$:Ce^{3+}, Tb^{3+} films.[34]

4. CONCLUSIONS

Crystalline $LaPO_4$:Ce^{3+} and $LaPO_4$:Ce^{3+}, Tb^{3+} nanoparticles with monoclinic monazite structure have been successfully prepared by the polyol method at 160 °C. The obtained nanoparticles have spherical morphology and narrow size distribution with an average size of around 20 nm, which can be dispersed in ethylene glycol to form a stable colloid solution. The doped rare earth ions (Ce^{3+}, Tb^{3+}) show their characteristic 5d–4f and f–f emission in $LaPO_4$ nanoparticles, respectively. An energy transfer from Ce^{3+} to Tb^{3+} has been observed in the Ce^{3+}, Tb^{3+}-codoped $LaPO_4$ nanoparticles as in the bulk materials. The energy-transfer efficiency increases with increasing the Tb^{3+} concentration when Ce^{3+} concentration is fixed.

Acknowledgments: This project is financially supported by the foundation of "Bairen Jihua" of the Chinese Academy of Sciences, the MOST of China (2003CB 314707), and the National Natural Science Foundation of China (NSFC, 20271048, 50225205, 20431030). Prof. J. Fang is grateful for the financial support by the foundation of a two-base program for international cooperation of NSFC (00310530) related to Project 50225205, and NSF DMR-0449580.

References and Notes

1. L. Yu, H. Song, S. Lu, Z. Liu, L. Yang, and X. Kong, *J. Phys. Chem. B* 108, 16697 (**2004**).
2. G. A. Hebbink, J. W. Stouwdam, D. N. Reinhoudt, and F. C. J. M. van Veggel, *Adv. Mater.* 14, 1147 (**2002**).
3. J. M. Tsay, M. Pflughoefft, L. A. Bentolila, and S. Weiss, *J. Am. Chem. Soc.* 126, 1926 (**2004**).
4. Y. Zhang and Y. Li, *J. Phys. Chem. B* 108, 17805 (**2004**).
5. N. Myung, Y. Bae, and A. J. Bard, *Nano. Lett.* 3, 747 (**2003**).
6. A. P. Alivisatos, *J. Phys. Chem.* 100, 13226 (**1996**).
7. A. Eychmüller, *J. Phys. Chem. B* 104, 6514 (**2000**).
8. H. Meyssamy, K. Riwotzki, A. Kornowski, S. Naused, and M. Haase, *Adv. Mater.* 11, 840 (**1999**).
9. M. Haase, K. Riwotzki, H. Meyssamy, and A. Kornowski, *J. Alloys Compounds* 303–304, 191 (**2000**).
10. K. Riwotzki, H. Meyssamy, A. Kornowski, and M. Haase, *J. Phys. Chem. B* 104, 2824 (**2000**).
11. K. Riwotzki, H. Meyssamy, H. Schnablegger, A. Kornowski, and M. Haase, *Angew. Chem. Int. Ed.* 40, 573 (**2001**).
12. C. Feldmann, *Adv. Funct. Mater.* 13, 101 (**2003**).
13. R. Bazzi, M. A. Flores, C. Louis, K. Lebbou, W. Zhang, C. Dujardin, S. Roux, B. Mercier, G. Ledoux, E. Bernstein, P. Perriat, and O. Tillement, *J. Colloid Interface Sci.* 273, 191 (**2004**).
14. K. Kömpe, H. Borchert, J. Storz, A. Lobo, S. Adam, T. Möller, and M. Haase, *Angew. Chem. Int. Ed.* 42, 5513 (**2003**).
15. V. Buissette, M. Moreau, T. Gacoin, J.-P. Boilot, J.-Y. Chane-Ching, and T. L. Mercier, *Chem. Mater.* 16, 3767 (**2004**).
16. O. Lehmann, K. Kömpe, and M. Haase, *J. Am. Chem. Soc.* 126, 14935 (**2004**).
17. C. Feldmann and C. Metzmacher, *J. Mater. Chem.* 11, 2603 (**2001**).
18. H.-O. Jungk and C. Feldmann, *J. Mater. Sci.* 36, 297 (**2001**).
19. L. K. Kurihara, G. M. Chow, and P. E. Schoen, *Nanostructured Mater.* 5, 607 (**1995**).
20. S. Sun, C. B. Murray, D. Weller, L. Folks, and A. Moser, *Science* 287, 1989 (**2000**).
21. C. Feldmann and H.-O. Jungk, *Angew. Chem. Int. Ed.* 40, 359 (**2001**).
22. C. Feldmann, *Scripta Mater.* 44, 2193 (**2001**).
23. E. W. Seelig, B. Tang, A. Yamilov, H. Cao, and R. P. H. Chang, *Mater. Chem. Phys.* 80, 257 (**2003**).
24. C. Feldmann and H.-O. Jungk, *J. Mater. Sci.* 37, 3251 (**2002**).
25. C. Feldmann, *Adv. Mater.* 13, 1301 (**2001**).
26. J. Merikhi, H.-O. Jungk, and C. Feldmann, *J. Mater. Chem.* 10, 1311 (**2000**).
27. R. C. Ropp, *J. Electrochem. Soc.: Solid State Sci.* 115, 841 (**1968**).
28. J. Dexpert-Ghys, R. Mauricot, and M. D. Faucher, *J. Lumin.* 69, 203 (**1996**).
29. R. P. Rao and D. J. Devine, *J. Lumin.* 87–89, 1260 (**2000**).
30. N. Hashimoto, Y. Takada, K. Sato, and S. Ibuki, *J. Lumin.* 48–49, 893 (**1991**).
31. S. Lucas, E. Champion, D. Bernache-Assollant, and G. Leroy, *J. Solid State Chem.* 177, 1312 (**2004**).
32. Y. W. Zhang, Y. Yang, S. Jin, S. J. Tian, G. B. Li, J. T. Jia, C. S. Liao, and C. H. Yan, *Chem. Mater.* 13, 372 (**2001**).
33. G. Blasse and A. Bril, *J. Chem. Phys.* 51, 3252 (**1969**).
34. M. Yu, J. Lin, J. Fu, H. J. Zhang, and Y. C. Han, *J. Mater. Chem.* 13, 1413 (**2003**).
35. J.-C. Bourcet and F. K. Fong, *J. Chem. Phys.* 60, 34 (**1974**).
36. M. T. Jose and A. R. Lakshmanan, *Opt. Mater.* 24, 651 (**2004**).
37. J. Y. Sun, H. Y. Du, and W. X. Hu, *Solid State Luminescent Materials* (*in Chinese*), Chemical Industry Press, Beijing (**2003**), p. 151.

Received: 30 December 2004. Accepted: 8 March 2005.

RESEARCH ARTICLE